Mineralogical Magazine (2024), **88**, 576–584
doi:10.1180/mgm.2024.40

CAMBRIDGE UNIVERSITY PRESS

Article

Sperlingite, $(H_2O)K(Mn^{2+}Fe^{3+})(Al_2Ti)(PO_4)_4[O(OH)][(H_2O)_9(OH)]\cdot 4H_2O$, a new paulkerrite-group mineral, from the Hagendorf-Süd pegmatite, Oberpfalz, Bavaria, Germany

Christian Rewitzer[1], Rupert Hochleitner[2], Ian E. Grey[3], Anthony R. Kampf[4], Stephanie Boer[5], Colin M. MacRae[3], William G. Mumme[3], Nicholas C. Wilson[3] and Cameron J. Davidson[3]

[1]Independent researcher, Graf von Bogen Str. 6, D-93437 Furth im Wald, Germany; [2]Mineralogical State Collection (SNSB), Theresienstrasse 41, 80333, München, Germany; [3]CSIRO Mineral Resources, Private Bag 10, Clayton South, Victoria 3169, Australia; [4]Mineral Sciences Department, Natural History Museum of Los Angeles County, 900 Exposition Boulevard, Los Angeles, CA 90007, USA; and [5]Australian Synchrotron, 800 Blackburn Road, Clayton, Victoria 3168, Australia

Abstract

Sperlingite, $(H_2O)K(Mn^{2+}Fe^{3+})(Al_2Ti)(PO_4)_4[O(OH)][(H_2O)_9(OH)]\cdot 4H_2O$, is a new monoclinic member of the paulkerrite group, from the Hagendorf-Süd pegmatite, Oberpfalz, Bavaria, Germany. It was found in corrosion pits of altered zwieselite, in association with columbite, hopeite, leucophosphite, mitridatite, scholzite, orange–brown zincoberaunite sprays and tiny green crystals of zincolibethenite. Sperlingite forms colourless prisms with pyramidal terminations, which are predominantly only 5 to 20 μm in size, rarely to 60 μm and frequently are multiply intergrown and are overgrown with smaller crystals. The crystals are flattened on {010} and slightly elongated along [100] with forms {010}, {001} and {111}. Twinning occurs by rotation about **c**. The calculated density is 2.40 g·cm^{-3}. Optically, sperlingite crystals are biaxial (+), $\alpha = 1.600$(est), $\beta = 1.615(5)$, $\gamma = 1.635(5)$ (white light) and 2V (calc.) = 82.7°. The optical orientation is $X = b$, $Y = c$ and $Z = a$. Neither dispersion nor pleochroism were observed. The empirical formula from electron microprobe analyses and structure refinement is $^{A1}[(H_2O)_{0.96}K_{0.04}]_{\Sigma 1.00}$ $^{A2}(K_{0.52}\square_{0.48})_{\Sigma 1.00}$ $^{M1}(Mn^{2+}_{0.60}Mg_{0.33}Zn_{0.29}Fe^{3+}_{0.77})_{\Sigma 1.99}$ $^{M2+M3}(Al_{1.05}Ti^{4+}_{1.33}Fe^{3+}_{0.62})_{\Sigma 3.00}(PO_4)_4$ $^{X}[F_{0.19}(OH)_{0.94}O_{0.87}]_{\Sigma 2.00}[(H_2O)_{9.23}(OH)_{0.77}]_{\Sigma 10.00}\cdot 3.96H_2O$. Sperlingite has monoclinic symmetry with space group $P2_1/c$ and unit-cell parameters $a = 10.428(2)$ Å, $b = 20.281(4)$ Å, $c = 12.223(2)$ Å, $\beta = 90.10(3)°$, $V = 2585.0(8)$ Å^3 and $Z = 4$. The crystal structure was refined using synchrotron single-crystal data to $wR_{obs} = 0.058$ for 5608 reflections with $I > 3\sigma(I)$. Sperlingite is the first paulkerrite-group mineral to have co-dominant divalent and trivalent cations at the *M*1 sites; All other reported members have Mn^{2+} or Mg dominant at *M*1. Local charge balance for Fe^{3+} at *M*1 is achieved by $H_2O \rightarrow OH^-$ at H_2O coordinated to *M*1.

Keywords: sperlingite; paulkerrite-group mineral; crystal structure; new mineral

(Received 14 March 2024; accepted 3 May 2024; Accepted Manuscript published online: 20 May 2024)

Introduction

Sperlingite was identified recently as a potential new mineral from scanning electron microscope and powder X-ray diffraction studies on a specimen collected at the Hagendorf-Süd feldspar mine by Christian Rewitzer in 1974. The mine has been a prolific source of new minerals, particularly secondary phosphate minerals, both during it's lifetime and after it's closure and flooding in 1984, when studies were continued on specimens in extensive collections from the mine, including those of Erich Keck (Birch *et al.*, 2018) and Gabriella K. Robertson (Mills *et al.*, 2016). Up to 1984, ten new minerals were published, including the phosphate minerals jungite, keckite, laueite, lehnerite, parascholzite, pseudolaueite, scholzite and wilhelmvierlingite as documented by Kastning and Schlüter (1994), while post 1984 another 23 type specimens have been added. Of particular relevance to this study is the characterisation of the paulkerrite-group minerals pleysteinite (Grey *et al.*, 2023a), hochleitnerite (Grey *et al.*, 2023b), rewitzerite (Grey *et al.*, 2023c) and fluor-rewitzerite (Hochleitner *et al.*, 2024). Their formulae and unit-cell parameters are given in Table 1. Pleysteinite and hochleitnerite were originally reported to be isostructural with orthorhombic (*Pbca*) benyacarite (Demartin *et al.*, 1993) based on laboratory-based sealed-tube single-crystal diffraction studies. A more recent study, however, using microfocus synchrotron diffraction data (Rewitzer *et al.*, 2024b) has confirmed that they have monoclinic symmetry, $P2_1/c$, and are isostructural with rewitzerite and fluor-rewitzerite. Sperlingite also has monoclinic symmetry and is the fifth member of the group to be described from Hagendorf-Süd. The mineral and its name (symbol Sper) have been approved by the Commission on New Minerals, Nomenclature and Classification (CNMNC) of the International Mineralogical Association (IMA), IMA2023–120 (Rewitzer *et al.*, 2024a). The name honours Thomas Sperling

Corresponding author: Ian E. Grey; Email: ian.grey@csiro.au
Associate Editor: Juraj Majzlan
Cite this article: Rewitzer C., Hochleitner R., Grey I.E., Kampf A.R., Boer S., MacRae C.M., Mumme W.G., Wilson N.C. and Davidson C.J. (2024) Sperlingite, $(H_2O)K(Mn^{2+}Fe^{3+})(Al_2Ti)(PO_4)_4[O(OH)][(H_2O)_9(OH)]\cdot 4H_2O$, a new paulkerrite-group mineral, from the Hagendorf-Süd pegmatite, Oberpfalz, Bavaria, Germany. *Mineralogical Magazine* **88**, 576–584. https://doi.org/10.1180/mgm.2024.40

Table 1. Monoclinic ($P2_1/c$) paulkerrite-group minerals from the Hagendorf-Süd pegmatite, Bavaria.

Pleysteinite	$[(H_2O)K]Mn_2Al_3(PO_4)_4F_2(H_2O)_{10}{\cdot}4H_2O$	a = 10.440(5), b = 20.588(5), c = 12.2341(3) Å β = 90.38(1)°	Rewitzer *et al.* (2024b)
Hochleitnerite	$[(H_2O)K]Mn_2(Ti_2Fe)(PO_4)_4O_2(H_2O)_{10}{\cdot}4H_2O$	a = 10.547(2), b = 20.577(4), c = 12.373(2) Å β = 90.09(3)°	Rewitzer *et al.* (2024b)
Rewitzerite	$[K(H_2O)]Mn_2(Al_2Ti)(PO_4)_4[O(OH)](H_2O)_{10}{\cdot}4H_2O$	$P2_1/c$, a = 10.444(2), b = 20.445(2), c = 12.269(1) Å β = 90.17(3)°	Grey *et al.* (2023c)
Fluor-rewitzerite	$[(H_2O)K]Mn_2(Al_2Ti)(PO_4)_4(OF)(H_2O)_{10}{\cdot}4H_2O$	a = 10.407(1), b = 20.514(2), c = 12.193(1) Å β = 90.49(2)°	Hochleitner *et al.* (2024)
Sperlingite	$[(H_2O)K](Mn^{2+}Fe^{3+})(Al_2Ti)(PO_4)_4[O(OH)][(H_2O)_9(OH)]{\cdot}4H_2O$	a = 10.428(2), b = 20.281(4), c = 12.223(2) Å β = 90.10(3)°	This study

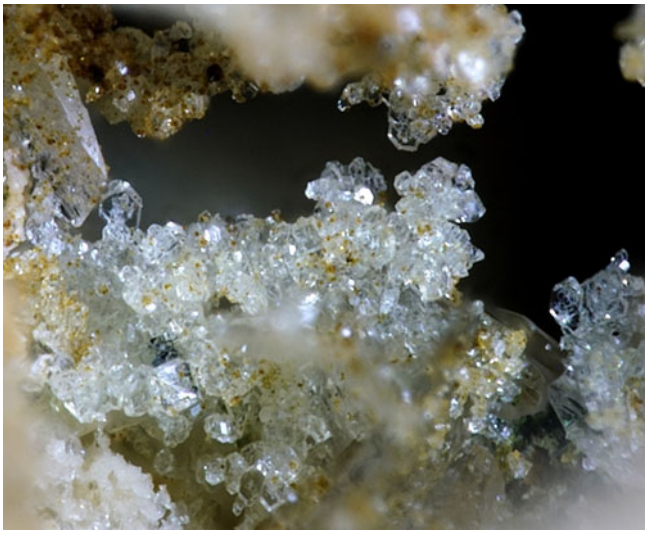

Figure 1. Aggregates of colourless sperlingite crystals in a corrosion pit in zwieselite associated with scholzite (large crystal in upper left). Photo by Christian Rewitzer, holotype specimen MSM38185, FOV = 0.3 mm.

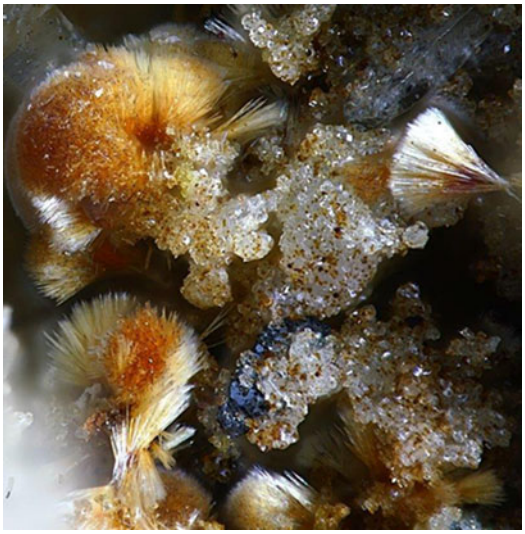

Figure 2. Aggregates of sperlingite crystals associated with sprays of zincoberaunite needles. Brown staining on sperlingite is mitridatite. Photo by Christian Rewitzer, holotype specimen MSM38185.

(born 1963) for his contributions to Bavarian mineralogy, especially in phosphates from the pegmatite of Hühnerkobel in the Bavarian Forest (Schaaf *et al.*, 2008). He is one of the best specialists in the history of Bavarian mineralogy (Sperling, 2000). Mr. Sperling has agreed to the mineral being named after him.

The holotype specimen is housed in the mineralogical collections of the Bavarian State Mineral Collection, Munich, registration number MSM38185. A cotype specimen used for the optical properties, powder X-ray diffraction and Raman spectrum is located at the Natural History Museum of Los Angeles County, catalogue number 76310.

Occurrence and associated minerals

The lead author (CR) found the specimen CR202, containing sperlingite, in mid 1974 on the mine dump at the Hagendorf Süd feldspar mine, in the Oberpfalz, northeast Bavaria, Germany (49°39′1″N, 12°27′35″E). Based on the time of collection, and the mineral associations in the specimen, particularly zinc-bearing minerals, the specimen most probably originated from the 67 m level of the mine (Mücke, 1981; Grey *et al.*, 2018). The matrix of the specimen consists of strongly corroded zwieselite residues in quartz, with clusters of sperlingite crystals occupying corrosion pits in the zwieselite (Fig. 1). Accompanying minerals are scholzite, hopeite, leucophosphite, orange–brown zincoberaunite sprays (Fig. 2), tiny green crystals of zincolibethenite, $CuZn(PO_4)(OH)$, olive green mitridatite and columbite. The colourless sperlingite crystals are commonly stained with mitridatite coatings (Figs 1 and 2). In addition to the close association of sperlingite with zwieselite, crystals are also observed growing on and within scholzite (Fig. 3). Sperlingite and scholzite are probably the youngest phosphate minerals in the specimen.

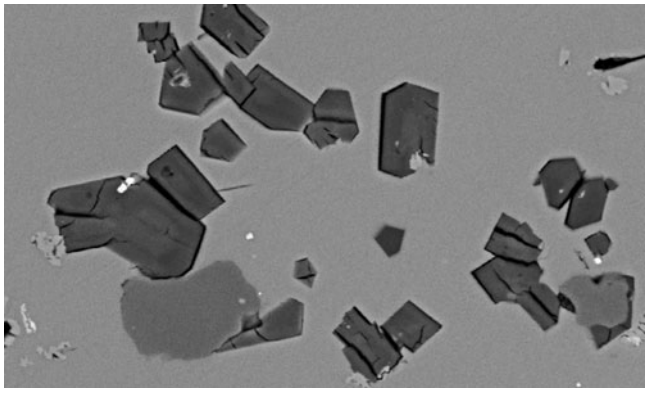

Figure 3. Back-scattered electron image of polished epoxy mount of holotype specimen MSM38185, used for EMP analyses, showing dark grey sperlingite crystals in a light grey scholzite matrix, associated with fluorapatite (medium grey). FOV = 80 μm.

https://doi.org/10.1180/mgm.2024.40 Published online by Cambridge University Press

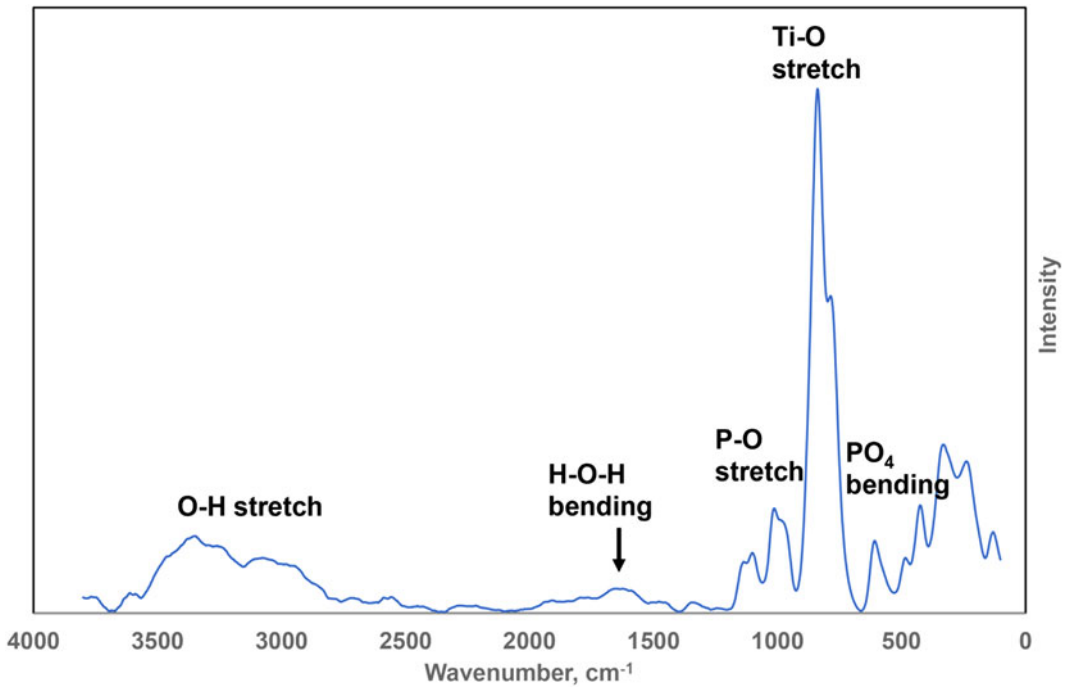

Figure 4. Raman spectrum of sperlingite.

Physical and optical properties

Crystals of sperlingite, in the form of colourless prisms with pyramidal terminations are predominantly only 5 to 20 μm in size (Fig. 3), rarely to 60 μm and are frequently multiply intergrown and overgrown with smaller crystals. The calculated density is 2.40 g·cm^{-3} for the empirical formula and single-crystal unit-cell parameters.

The small size of the sperlingite crystals limited the measurement of the optical properties; however, it was possible to measure two indices of refraction in grain mounts. Based upon these and by comparison with the optical properties and morphologies of other paulkerrite-group minerals, it was possible to conjecture the following properties: biaxial (+), $\alpha = 1.600$(est), $\beta = 1.615(5)$, $\gamma = 1.635(5)$ (white light) and 2V (calc.) = 82.7°. The optical orientation is $X = b$, $Y = c$ and $Z = a$. Neither dispersion nor pleochroism were observed.

Table 2. Analytical data (wt.%) for sperlingite.

	Sperlingite Average of 11 analyses			Rewitzerite Grey *et al.* (2023c)	
Const.	Mean	Range	S.D.		Standard
K_2O	2.78	2.14–3.65	0.50	3.93	Adularia
MnO	4.56	3.65–5.79	0.72	6.33	$MnSiO_3$
MgO	1.42	0.72–2.54	0.64	2.80	Spinel
ZnO	2.51	0.69–4.41	0.93	-	Sphalerite
Al_2O_3	5.69	3.32–8.29	1.63	8.37	Berlinite
Fe_2O_3	11.77	7.81–14.51	2.22	7.44	Hematite
TiO_2	11.28	8.79–14.08	1.64	9.18	Rutile
P_2O_5	30.21	26.63–32.84	1.76	30.90	Berlinite
F	0.39	0.00–0.92	0.34	0.87	Fluorite
H_2O_{calc}*	28.74			30.39	
–O≡F	–0.16			–0.37	
Total	99.19			99.84	

* Based on the ideal formula: 14 $H_2O + 2OH^-$ per 4P.

Raman spectroscopy

Raman spectroscopy was conducted on a Horiba XploRA PLUS spectrometer using a 532 nm diode laser, 100 μm slit and 1800 gr/mm diffraction grating and a 100× (0.9 NA) objective. The spectrum is shown in Fig. 4. The O–H stretch region has a broad double hump that can be assigned to H-bonded water, with maxima at 3338 and 3057 cm^{-1}. According to Libowitzky (1999) these correspond to O···O distances involved in H-bonding of 2.65 and 2.75, corresponding to moderately strong H-bonding. Hydroxyl ion stretching is evident by a weak peak at 3600 cm^{-1}. The H–O–H bending mode region for water has a

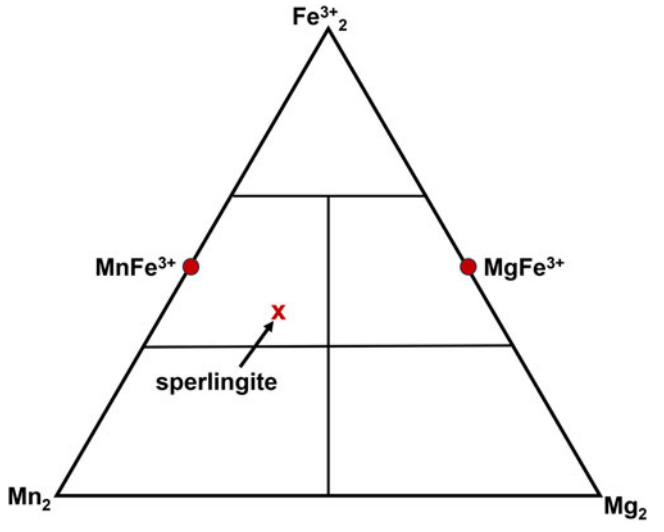

Figure 5. ternary diagram for $(M1)_2$ site Mn^{2+}–Mg–Fe^{3+} compositions, showing end-member compositions and location of the empirical composition for sperlingite. Note that the divalent cations correspond to the dominant cations found at *M*1 in paulkerrite-group minerals.

https://doi.org/10.1180/mgm.2024.40 Published online by Cambridge University Press

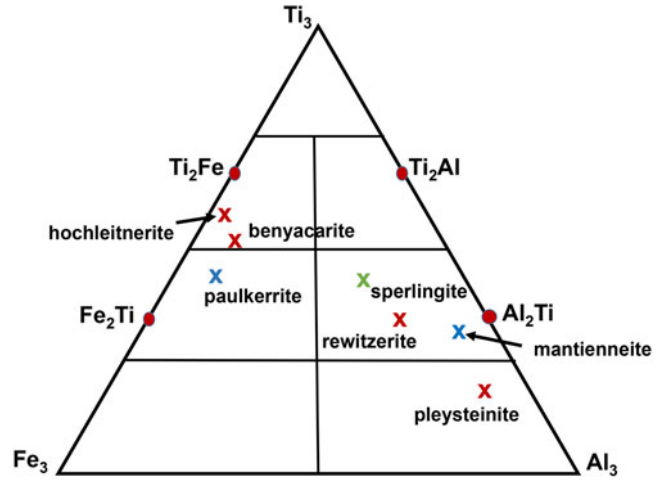

Figure 6. Ternary diagram for $(M2)_2M3$ site Al–Ti–Fe^{3+} compositions, showing end-member compositions (Al_2Ti, Ti_2Al etc.) and location of the empirical composition for sperlingite. For comparison the published empirical compositions are shown for the paulkerrite-group minerals benyacarite (Demartin *et al.*, 1993,1997), paulkerrite (Peacor *et al.*, 1984), mantienneite (Fransolet *et al.*, 1984), rewitzerite (Grey *et al.*, 2023a), pleysteinite (Grey *et al.*, 2023c) and hochleitnerite (Grey *et al.*, 2023d). Red crosses correspond to minerals with Mn at *M*1 and blue crosses correspond to minerals with Mg at *M*1.

peak at 1630 cm^{-1}. Two peaks at 1012 and 965 cm^{-1} in the P–O stretching region can be assigned to symmetric stretching modes whereas weaker peaks at 1135 and 1100 cm^{-1} correspond to anti-symmetric P–O stretching modes. Bending mode vibrations of the $(PO_4)^{3-}$ groups are located at 610 cm^{-1} and at 485 and 425 cm^{-1}. Peaks at lower wavenumbers are related to lattice vibrations. The spectrum for sperlingite is dominated by a strong peak at 838 cm^{-1} with a shoulder at 785 cm^{-1}. These peaks are present in all paulkerrite-group minerals (Grey *et al.*, 2023a–c) and can be assigned to Ti–O stretch vibrations for short Ti–O bonds that occur in linear trimers of corner-connected octahedra *M*2–*M*3–*M*2 in the structure, by analogy with published Raman spectra for titanates containing short Ti–O distances (Tu *et al.*, 1996; Bamberger *et al.*, 1990; Silva *et al.*, 2018).

Chemical composition

Highly hydrated paulkerrite-group minerals present problems for analysis because of dehydration in the high vacuum of the conductive film coater and the microprobe, resulting in severe cracking and high analysis totals (Sejkora *et al.*, 2006). Cracking of crystals of sperlingite during coating of a conductive iridium film is seen in the polished section used for the electron microprobe analyses in Fig. 3. To prevent further dehydration during analysis a cold stage cooled to liquid nitrogen temperature was employed in the microprobe and the specimen was precooled under dry nitrogen prior to introduction to the microprobe vacuum.

Crystals of sperlingite were analysed using wavelength-dispersive electron microprobe (EMP) spectrometry on a JEOL JXA 8530F Hyperprobe operated at an accelerating voltage of 15 kV and a beam current of 2.0 nA. The beam was defocused to typically ~5 μm. Both specimen and standards were coated with a 25 Å thick film of iridium for the analyses. The F *K* peak was partially overlapped by Mn *L* and Fe *L* and this was corrected using a peak overlap procedure. In addition the thin film correction procedure was utilised in *STRATA* (Pouchou, 1993) to remove the effects of the Ir coating. There was insufficient material for direct determination of H_2O, so it was calculated based on the ideal formula (14 $H_2O + 2OH^-$ per 4 P). Analytical results (average of 11 analyses on 11 crystals) are

Table 3. Powder X-ray diffraction data (*d* in Å) for sperlingite (I_{calc} > 1.5)*.

I_{obs}	d_{obs}	d_{calc}	I_{calc}	*h k l*	I_{obs}	d_{obs}	d_{calc}	I_{calc}	*h k l*	I_{obs}	d_{obs}	d_{calc}	I_{calc}	*h k l*
37	**10.236**	**10.141**	**47**	**0 2 0**	16	2.648	2.638	4	$\bar{2}$ 0 4	6	1.777	1.759	6	$\bar{3}$ 0 6
52	**7.447**	**7.383**	**58**	**1 1 1**	22	2.596	2.594	14	3 4 2			1.751	2	$\bar{4}$ 7 3
100	**6.176**	**6.112**	**100**	**0 0 2**			2.572	10	2 6 2	13	1.695	1.710	3	4 6 4
		5.277	2	$\bar{1}$ 0 2	11	2.549	2.550	2	2 2 4			1.690	9	0 12 0
35	**5.191**	**5.214**	**22**	**2 0 0**			2.529	14	4 1 1	16	1.660	1.676	2	5 7 1
		5.147	8	$\bar{1}$ 3 1	14	2.492	2.516	2	2 5 3			1.662	2	$\bar{3}$ 4 6
		5.070	12	0 4 0			2.480	9	$\bar{2}$ 7 1			1.654	5	2 6 6
13	4.704	4.675	3	1 2 2			2.461	5	3 3 3			1.650	2	$\bar{6}$ 2 2
		4.637	7	2 2 0	10	2.353	2.342	3	0 8 2			1.644	5	6 4 0
22	3.964	3.963	5	2 0 2			2.335	3	$\bar{4}$ 2 2			1.629	2	0 12 2
		3.910	24	2 3 1	10	2.302	2.297	4	$\bar{3}$ 0 4	16	1.602	1.608	3	2 12 0
41	**3.727**	**3.732**	**4**	**$\bar{1}$ 1 3**			2.284	5	1 8 2			1.601	3	4 10 0
		3.697	37	$\bar{2}$ 2 2	11	2.175	2.169	4	$\bar{4}$ 4 2			1.587	9	$\bar{4}$ 2 6
		3.635	6	2 4 0			2.159	2	$\bar{4}$ 5 1	8	1.559	1.548	7	4 10 2
6	3.379	3.380	4	0 6 0			2.105	2	$\bar{2}$ 3 5			1.518	3	4 7 5
		3.311	3	$\bar{1}$ 3 3	13	2.065	2.080	2	$\bar{2}$ 6 4	8	1.492	1.510	2	6 0 4
		3.126	2	$\bar{2}$ 4 2			2.064	3	4 6 0			1.494	2	$\bar{4}$ 11 1
86	**3.101**	**3.096**	**46**	**2 5 1**			2.037	8	0 0 6			1.479	3	0 12 4
		3.056	20	0 0 4	8	1.987	1.982	4	4 0 4	13	1.455	1.463	2	0 4 8
		3.024	9	$\bar{3}$ 0 2	18	1.961	1.957	14	$\bar{4}$ 6 2			1.449	6	$\bar{6}$ 4 4
35	**2.979**	**2.998**	**2**	**$\bar{3}$ 3 1**			1.942	5	3 8 2			1.437	2	0 10 6
		2.958	9	0 6 2	11	1.910	1.914	2	$\bar{4}$ 7 1	6	1.407	1.417	2	4 3 7
		2.934	14	$\bar{1}$ 0 4			1.890	6	0 4 6			1.396	2	2 14 0
13	2.891	2.894	6	3 2 2	10	1.869	1.866	6	$\bar{2}$ 2 6					
43	**2.839**	**2.836**	**24**	**2 6 0**			1.848	5	5 1 3					
		2.818	8	$\bar{1}$ 2 4	8	1.819	1.828	2	$\bar{2}$ 8 4					
		2.772	11	$\bar{1}$ 5 3			1.805	5	2 10 2					

*The strongest lines are given in bold.

https://doi.org/10.1180/mgm.2024.40 Published online by Cambridge University Press

Table 4. Crystal data and structure refinement for sperlingite.

Crystal data	
Ideal formula	$(H_2O)K(MnFe^{3+})Al_2Ti(PO_4)_4[(H_2O)_9(OH)]\cdot 4H_2O$
Formula weight	933.6
Symmetry, space group	Monoclinic, $P2_1/c$ (#14)
Unit-cell dimensions	a = 10.428(2), b = 20.281(4), c = 12.223(2) Å β = 90.10(3)°
Volume, Z	2585.0(8) Å^3, 4
Data collection	
Data collection	Synchrotron Microfocus beamline
Wavelength, temperature	0.7109 Å, 100 K
Crystal size (mm)	0.020 × 0.020 × 0.010
Absorption correction	Multiscan, T_{min} 0.42, T_{max} 0.75
Twinning	2-fold rotation about **c**. Twin volumes 0.528(3), 0.472(3)
θ range for data collection	1.95 to 32.06°
Index ranges	$-14 \le h \le 14$, $-30 \le k \le 30$, $-16 \le l \le 16$
Refl. collected, independent	44006, 7137
Reflections with $I_o > 3\sigma(I)$	5608
Refinement	
Refinement method	Full-matrix least-squares on F
Data/ constraints/ parameters	7122/0/390
Final R indices [$I > 3\sigma(I)$]	R_{obs} = 0.050, *wR_{obs} = 0.058
R indices (all data)	R_{obs} = 0.063, wR_{obs} = 0.059
Goodness of Fit	2.80
Largest diff. peak and hole	1.07 and −0.78 e$^-$.Å^2

*$w = [\sigma^2(|F_o|)+(uF_o)^2]^{-1}$, u = instability factor

Table 5. Refined atom coordinates, site scattering (electrons), equivalent isotropic displacement parameters (Å^2) and bond valence sums (BVS, in valence units) for sperlingite.

Atom	x	y	z	U_{eq}	BVS
*M*1a	0.49776(7)	0.74704(3)	0.24426(6)	0.0304(2)	2.44
*M*1b	0.99733(8)	−0.24677(4)	−0.24235(7)	0.0321(3)	2.41
*M*2a	0.66013(11)	0.50295(4)	0.74325(8)	0.0279(3)	3.56
*M*2b	1.16103(12)	−0.00360(4)	−0.74169(10)	0.0396(4)	3.65
*M*3a	0.5	0.5	0.5	0.0293(4)	3.96
*M*3b	1	0	−0.5	0.0386(5)	4.15
P1a	0.90979(14)	0.59578(5)	0.80203(11)	0.0306(4)	5.08
P1b	1.40937(13)	−0.09537(5)	−0.80165(10)	0.0260(3)	5.07
P2a	0.58744(14)	0.59102(6)	0.29672(10)	0.0264(3)	5.13
P2b	1.08535(14)	−0.09004(6)	−0.29621(12)	0.0304(4)	4.99
*A*1	0.7222(3)	0.85361(13)	0.0544(2)	0.0401(10)	0.04
*A*2	1.2241(2)	−0.35214(9)	−0.0565(2)	0.0414(7)	0.48
*X*1	0.6411(5)	0.50256(14)	0.5980(3)	0.0288(10)	1.64
*X*2	1.1406(4)	−0.00330(13)	−0.5977(3)	0.0275(9)	1.73
O1a	0.9068(3)	0.67059(13)	0.8053(3)	0.0371(11)	1.80
O1b	1.4026(3)	−0.17065(15)	−0.8047(3)	0.0350(10)	1.74
O2a	1.0286(3)	0.57105(15)	0.7387(3)	0.0312(11)	1.80
O2b	1.5281(3)	−0.07302(14)	−0.7390(3)	0.0311(11)	1.81
O3a	0.9092(4)	0.56747(13)	0.9179(3)	0.0328(11)	1.94
O3b	1.4120(3)	−0.06857(15)	−0.9191(3)	0.0298(10)	1.91
O4a	0.7881(3)	0.57239(16)	0.7440(3)	0.0349(11)	1.87
O4b	1.2866(3)	−0.07183(16)	−0.7445(3)	0.0320(11)	1.96
O5a	0.5967(3)	0.66597(14)	0.2903(3)	0.0332(10)	1.76
O5b	1.0927(3)	−0.16515(14)	−0.2882(3)	0.0383(11)	1.77
O6a	0.4677(3)	0.56553(15)	0.2383(3)	0.0293(10)	1.87
O6b	0.9655(3)	−0.06647(14)	−0.2335(3)	0.0339(11)	1.79
O7a	0.5830(4)	0.56962(15)	0.4157(3)	0.0314(10)	1.96
O7b	1.0822(4)	−0.06751(13)	−0.4163(3)	0.0319(10)	2.03
O8a	0.7080(3)	0.56379(15)	0.2411(3)	0.0297(10)	1.85
O8b	1.2077(4)	−0.06243(15)	−0.2424(3)	0.0374(12)	1.86
O9a	0.3509(4)	0.68932(17)	0.1802(3)	0.0422(12)	0.43
O9b	0.8502(3)	−0.18783(17)	−0.1824(3)	0.0412(12)	0.42
O10a	0.5834(3)	0.74189(17)	0.0852(3)	0.0357(11)	0.37
O10b	1.0803(4)	−0.24262(17)	−0.0820(4)	0.0417(12)	0.45
O11a	0.6437(4)	0.80461(18)	0.3084(4)	0.0459(13)	0.43
O11b	1.1438(3)	−0.30618(16)	−0.3093(3)	0.0384(11)	0.40
O12a	0.4099(3)	0.75085(16)	0.4012(3)	0.0373(11)	0.42
O12b	0.9106(4)	−0.25223(18)	−0.4035(4)	0.0435(13)	0.34
O13a	0.6619(5)	0.50291(15)	0.9133(3)	0.0378(12)	0.40
O13b	1.1642(5)	−0.00345(15)	−0.9125(3)	0.0360(11)	0.39
O14a	0.2636(4)	0.64214(15)	0.4400(3)	0.0456(13)	0.01
O14b	0.7644(3)	−0.14295(15)	−0.4381(3)	0.0429(12)	0.01
O15a	0.5362(3)	0.40625(15)	1.0122(3)	0.0451(8)	0.08
O15b	1.0128(4)	0.0965(3)	−1.0007(3)	0.0708(14)	0.02

given in Table 2, where they are compared with the published analyses for rewitzerite (Grey *et al.*, 2023c). Relatively high standard deviations are due to chemical zoning of the crystals, shown by variations in back-scatter contrast in Fig. 3. The EMP results show strong positive correlations of Al with F ($R^2 = 0.83$) and with K ($R^2 = 0.78$) and negative correlations of Ti with K ($R^2 = 0.86$) and with F ($R^2 = 0.73$). Al correlates negatively with Fe ($R^2 = 0.76$). (Mg + Zn) has a moderate negative correlation with Fe ($R^2 = 0.61$).

From the mean analyses, the number of atoms per formula unit (apfu), normalised to 4P apfu is:

$$K_{0.56}Mn_{0.60}Mg_{0.33}Zn_{0.29}Fe^{3+}_{1.39}Al_{1.05}Ti_{1.33}P_{4.00}F_{0.19}O_{32.73}H_{30.00}.$$

Expressing the apfu in structural form and allowing for local charge balance for Fe^{3+} at *M*1, by replacing an equivalent amount of H_2O coordinated to *M*1 with OH^-, according to the model proposed for sigloite by Hawthorne (1988) gives the following empirical formula. The *M*2 and *M*3 sites are grouped based on the site-total-charge procedure (Bosi *et al.*, 2019a, 2019b; Grey *et al.* 2023d):

$$^{A1}[(H_2O)_{0.96}K_{0.04}]_{\Sigma 1.00}\ ^{A2}(K_{0.52}W_{0.48})_{\Sigma 1.00}\ ^{M1}(Mn^{2+}_{0.60}Mg_{0.33}Zn_{0.29}Fe^{3+}_{0.77})_{\Sigma 1.99}\ ^{M2+M3}(Al_{1.05}Ti^{4+}_{1.33}Fe^{3+}_{0.62})_{\Sigma 3.00}(PO_4)_4\ ^{X}[F_{0.19}(OH)_{0.94}O_{0.87}]_{\Sigma 2.00}[(H_2O)_{9.23}(OH)_{0.77}]_{\Sigma 10.00}\cdot 3.96H_2O$$

The simplified formula is

$$(H_2O)(K, \square)(Mn^{2+}, Mg, Zn, Fe^{3+})_2(Al, Ti^{4+}, Fe^{3+})_3(PO_4)_4[F, (OH), O]_2[H_2O, OH]_{10}\cdot 4H_2O$$

The ideal formula is $(H_2O)K(Mn^{2+}Fe^{3+})(Al_2Ti)(PO_4)_4[O(OH)][(H_2O)_9(OH)]\cdot 4H_2O$, which requires K_2O 5.04, MnO 7.60, Al_2O_3 10.92, P_2O_5 30.41, TiO_2 8.56, Fe_2O_3 8.55, H_2O 28.92, total 100.00 wt.%.

Note that the *M*1 site has similar levels of divalent (1.22 apfu) and trivalent (0.77 apfu) cations, and the dominant divalent cation is Mn^{2+}, giving the end-member *M*1 (=*M*1a+*M*1b) site composition as ($Mn^{2+}Fe^{3+}$), illustrated in Fig. 5, while the merged (*M*2$_2$*M*3) site composition corresponds to the end-member composition (Al_2Ti) as shown in Fig. 6.

Crystallography

Powder X-ray diffraction data were obtained using a Rigaku R-AXIS Rapid II curved imaging plate microdiffractometer, with monochromatised Mo*K*α radiation. Observed *d* values and intensities were derived by profile fitting using JADE Pro software. Data (in Å for Mo*K*α) are given in Table 3. Refined monoclinic (space group: $P2_1/c$ (#14)) unit cell parameters from the powder data using *JADE Pro* with whole pattern fitting are

https://doi.org/10.1180/mgm.2024.40 Published online by Cambridge University Press

Table 6. Refined site occupancies and site scattering for sperlingite.

Site	Site scattering used in refinement	Scattering
*M*1a	0.929(6) Mn* + 0.071 Mg	24.07
*M*1b	0.801(6) Mn + 0.199 Mg	22.41
*M*2a	0.31 Fe + 0.40(1) Al + 0.29 Ti	19.64
*M*2b	0.31 Fe + 0.38(1) Al + 0.31 Ti	19.82
*M*3a	0.26(1) Al + 0.74 Ti	19.66
*M*3b	0.23(1) Al + 0.77 Ti	19.93
*A*1	0.145(8) K + 0.855 O	9.59
*A*2	0.512(4) K + 0.488 □	9.73

*Mn scattering curve used for Mn+Fe+Zn

$a = 10.43(3)$ Å, $b = 20.28(3)$ Å, $c = 12.22(3)$ Å, $\beta = 90.1(6)°$, $V = 2585(10)$ Å^3 and $Z = 4$.

A crystal measuring $0.020 \times 0.020 \times 0.010$ mm was used for a data collection at the Australian Synchrotron microfocus beamline MX2 (Aragao *et al*., 2018). Intensity data were collected using a Dectris Eiger 16M detector and monochromatic radiation with a wavelength of 0.7109 Å. The crystal was maintained at 100 K in an open-flow nitrogen cryostream during data collections. The diffraction data were collected using a single 36 second sweep of 360° rotation around phi. The resulting dataset consists of 3600 individual images with an approximate phi angle of each image being 0.1 degrees. The raw intensity dataset was processed using *XDS* software (Kabsch, 2010) to produce data files that were analysed using *SHELXT* (Sheldrick, 2015) and *JANA2006* (Petříček *et al*., 2014). Refined unit-cell parameters and other data collection conditions are given in Table 4.

Structure refinement

A structural model for sperlingite was obtained in space group $P2_1/c$ using *SHELXT* (Sheldrick, 2015). The *SHELXT* model had the same structure as for rewitzerite (Grey *et al*., 2023c) and so the rewitzerite coordinate file was used to initiate the refinement to ensure the same atom labelling. Twinning was implemented with 2-fold rotation about **c**. To establish site scattering at the *M*1 to *M*3 sites, pairs of light and heavy elements were incorporated at the sites and their occupancies were refined; Mn + Mg at *M*1 and Ti + Al at *M*2 and *M*3. Initially K plus O (for H_2O) were incorporated at the *A* sites with full occupancy, but refinement of their relative amounts gave a K content considerably lower than the EMP value. Next, vacancies were introduced to increase the K content, but with 3 components at the *A* sites, the site compositions are indeterminate. The simplest model, with only two components at each site, was to have K plus vacancies at the site with the higher scattering, and H_2O plus K at the other. This gave 0.66 K apfu, which is within the range of EMP analyses for K. After preliminary refinements, the program *OccQP* (Wright *et al*., 2000) was applied to optimise the site occupancies based on the empirical formula together with refined bond distances and site scattering. The output from *OccQP* had only Al and Ti at the *M*3 sites, but Al, Ti and Fe at the *M*2 sites. The *M*2 site occupancies were then modified to include a fixed amount of Fe (0.31 Fe per site) with refinement of Al and Ti. A pleasing result from this refinement was that the total Al and Ti contents from refinement of the occupancies at the *M*2 and *M*3 sites agreed with the values from the EMP analyses.

Refinement with anisotropic displacement parameters in *JANA2006* converged at $R_{obs} = 0.050$ for 5608 reflections with $I > 3\sigma(I)$. Difference-Fourier maps were used to search for H atoms but unambiguous locations could not be established. This is most likely because the chemical zoning caused local atomic shifts of the oxygen atoms in response to different elements at metal atom sites, which is reflected in high atomic displacement parameters as shown in Table 5. Details of the data collection and refinement are given in Table 4. The refined coordinates, equivalent isotropic displacement parameters and bond valence sum (BVS) values (Gagné and Hawthorne, 2015) are reported in Table 5. For the *M*1 sites, the BVS values were calculated based on the site occupancy in the empirical formula, $0.30Mn^{2+} + 0.165Mg + 0.145Zn + 0.39Fe^{3+}$. For the *M*2, *M*3 and

Table 7. Polyhedral bond lengths [Å] for sperlingite.

Bond	Length	Bond	Length	Bond	Length	Bond	Length
*M*1a–O1b	2.032(3)	*M*1b–O1a	2.010(3)	*A*1–*X*1	3.084(4)	P1a–O1a	1.518(3)
*M*1a–O5a	2.021(3)	*M*1b–O5b	2.012(3)	*A*1–O4a	2.845(5)	P1a–O2a	1.545(4)
*M*1a–O9a	2.080(4)	*M*1b–O9b	2.080(3)	*A*1–O7a	2.720(4)	P1a–O3a	1.528(4)
*M*1a–O10a	2.143(4)	*M*1b–O10b	2.142(5)	*A*1–O9b	3.297(5)	P1a–O4a	1.528(4)
*M*1a–O11a	2.071(4)	*M*1b–O11b	2.112(4)	*A*1–O10a	2.715(4)	<P1a–O>	1.530
*M*1a–O12a	2.129(4)	*M*1b–O12b	2.169(4)	*A*1–O11a	3.363(5)		
<*M*1a–O>	2.079	<*M*1b–O>	2.087	*A*1–O12b	2.890(4)	P1b–O1b	1.529(3)
				*A*1–O15b	3.016(6)	P1b–O2b	1.523(4)
*M*2a–*X*1	1.782(3)	*M*2b–*X*2	1.772(4)	<*A*1–*X*,O>	2.991	P1b–O3b	1.535(3)
*M*2a–O2b	1.991(3)	*M*2b–O2a	1.958(3)			P1b–O4b	1.536(3)
*M*2a–O4a	1.940(3)	*M*2b–O4b	1.905(3)	*A*2–*X*2	3.099(3)	<P1b–O>	1.531
*M*2a–O6a	1.939(3)	*M*2b–O6b	1.963(3)	*A*2–O4b	2.844(4)	O11a··O2b	2.819
*M*2a–O8b	1.913(3)	*M*2b–O8a	1.932(3)	*A*2–O7b	2.791(4)	P2a–O5a	1.525(3)
*M*2a–O13a	2.079(4)	*M*2b–O13b	2.088(4)	*A*2–O9a	3.288(5)	P2a–O6a	1.527(3)
<*M*2a–*X*,O>	1.941	<*M*2–*X*,O>	1.936	*A*2–O10b	2.698(4)	P2a–O7a	1.518(3)
				*A*2–O11b	3.333(5)	P2a–O8a	1.533(4)
*M*3a–*X*1 ×2	1.897(4)	*M*3b–*X*2 ×2	1.894(4)	*A*2–O12a	2.871(4)	<P2a–O>	1.526
*M*3a–O3b ×2	1.938(3)	*M*3b–O3a ×2	1.942(3)	*A*2–O15a	2.781(5)		
*M*3a–O7a ×2	1.951(3)	*M*3b–O7b ×2	1.912(3)	<*A*2–*X*,O>	2.963	P2b–O5b	1.528(3)
<*M*3a–*X*,O>	1.929	<M3b–*X*,O>	1.916			P2b–O6b	1.541(4)
						P2b–O7b	1.538(4)
						P2b–O8b	1.540(4)
						<P2b–O>	1.537

https://doi.org/10.1180/mgm.2024.40 Published online by Cambridge University Press

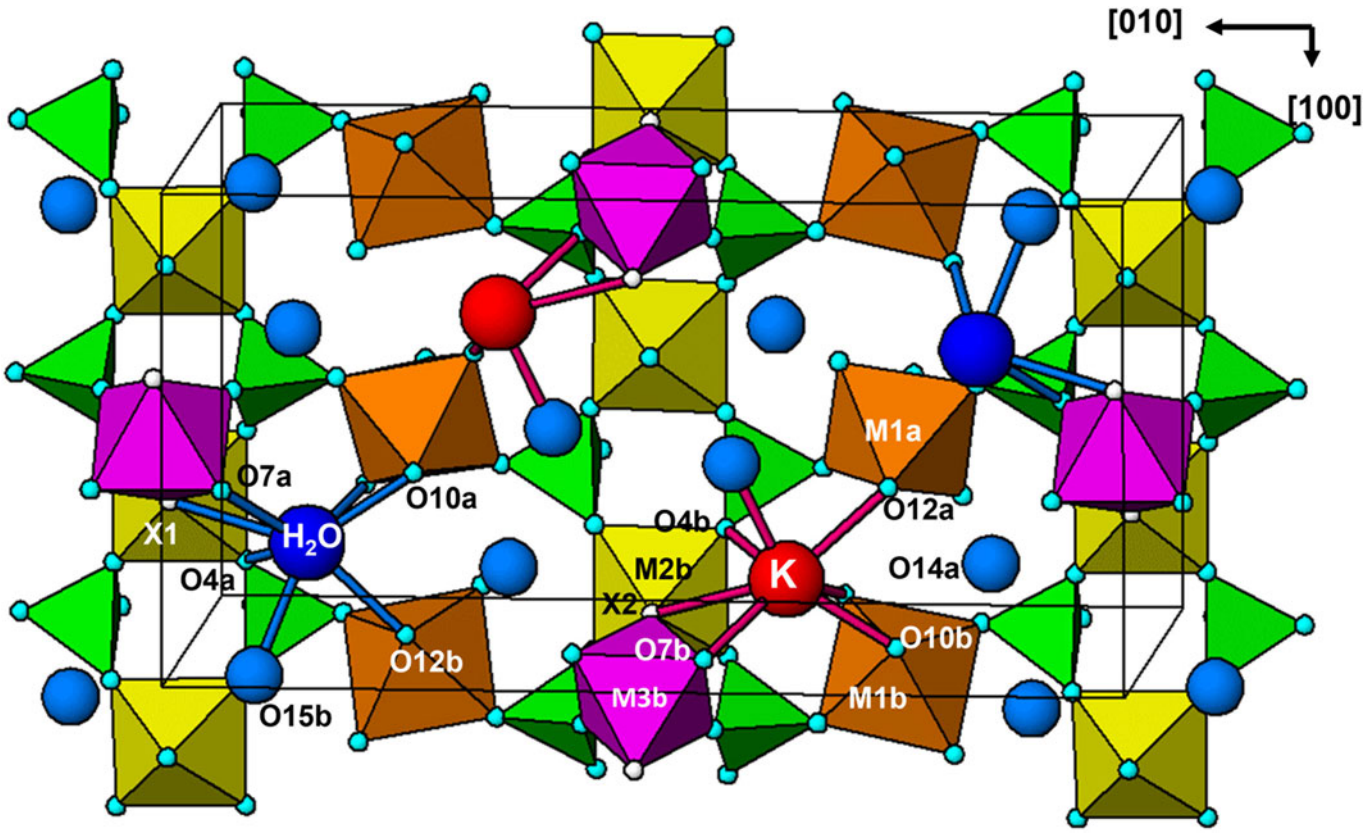

Figure 7. (001) section through the sperlingite crystal structure at $z = ¼$. Atom labelling consistent with Table 5, with K at *A*2 and H_2O at *A*1 sites. Prepared using *ATOMS* (Dowty, 2004).

A sites the BVS values were calculated using the refined site occupancies as listed in Table 6. Selected interatomic distances are reported in Table 7. The crystallographic information file has been deposited with the Principal Editor of *Mineralogical Magazine* and is available as Supplementary material (see below).

Although the H atoms in sperlingite could not be located during the refinement, we have located the majority of H atoms in refinements of the isostructural minerals fluor-rewitzerite (Hochleitner *et al.*, 2024) and macraeite (Grey *et al.*, 2024) and have established the H-bonding in these paulkerrite-group minerals. There is good agreement between the H-bonding schemes for the two minerals and also with that reported for benyacarite (Demartin *et al.*, 1993). Applying this information to sperlingite, the O···O pairs involved in hydrogen bonding are listed in Table 8, together with bond valences, *s*, calculated from O···O using the Ferraris and Ivaldi (1988) formula $s = [(O\cdots O)/2.17]^{-8.2} + 0.06$. The contributions to the BVS from the H bonds, as listed in Table 8, complement reasonably the undersaturated BVS values for the acceptor anions, O1 to O8, in Table 5.

Description of the structure

The crystal structure for sperlingite is based on an open 3D framework of corner-connected octahedra and tetrahedra of composition $[(MnFe^{3+})(Al_2Ti)(PO_4)_4O_2(H_2O)_{10}]^{1-}$, with water molecules and K^+ ions occupying <110> channels in the framework. Although H atoms were not located in the refinement the BVS values in Table 5 show that O9 to O15 are H_2O, as well as the main constituent at *A*1. The groups O9 to O12 are coordinated to *M*1 and O13 is coordinated to *M*2. The framework is built from heteropolyhedral layers parallel to (001) and located at $z = ¼$ and ¾, shown in Fig. 7, that are interconnected by corner-sharing of $M2O_4X(H_2O)$ octahedra with $M3O_4X_2$ octahedra located at $z = 0$ and ½. The heteropolyhedral (001) layers are built from [100] kröhnkite-type chains (Hawthorne, 1985) of 4-member rings of corner-connected PO_4 tetrahedra and $M2O_4X(H_2O)$ octahedra. Each PO_4 tetrahedron also shares a corner with $M1O_2(H_2O)_4$ octahedra along [010]. The corner-shared linkages form 8-member rings of alternating octahedra and tetrahedra. The *A*1 (H_2O) and *A*2 (K) sites are located in the 8-member rings as shown in Fig. 7.

The major difference between the crystal structure of sperlingite and that of orthorhombic paulkerrite-group minerals such as benyacarite (Demartin *et al.*, 1993) is an ordering of H_2O and K at the *A*1 and *A*2 sites, whereas they are disordered at a single *A* site in benyacarite. The different coordination environments at *A*1 and *A*2 are compared in Table 7 and shown in Fig. 7. The coordinations are very similar, except for the bond to O15, with the K-containing *A*2 site having a distance to O15a that is 0.24 A shorter than the *A*1–O15b distance. The same large difference in *A*-O15 distances is observed for other monoclinic paulkerrite-group minerals, rewitzerite (Grey *et al.*, 2023c) and paulkerrite (Grey *et al.*, 2023d).

Discussion

The general formula for monoclinic paulkerrite-group minerals is $A1A2M1_2M2_2M3(PO_4)_4X_2(H_2O)_{10}\cdot 4H_2O$. Sperlingite is the first

https://doi.org/10.1180/mgm.2024.40 Published online by Cambridge University Press

Table 8. H-bonding in sperlingite.

Donor···Acceptor	O···O (Å)	Bond valence[1]
O9a···O5b	2.764	0.198
O9a···O6a	2.879	0.158
O9a···O1b	2.896	0.154
O9b···O5a	2.7	0.227
O9b···O6b	2.81	0.180
O10a···O12a	2.887	0.156
O10a···O14b	2.77	0.195
O10b···O12b	2.814	0.179
O10b···O14a	2.807	0.181
O11a···O1a	2.79	0.187
O11a···O4a	3.019	0.127
O11a···O2b	2.819	0.177
O11b···O1b	2.739	0.208
O11b···O2a	2.827	0.174
O11b···O4b	2.993	0.132
O12a···O14a	2.723	0.215
O12b···O14b	2.723	0.215
O12b···A1	2.89	0.155
O13a···O15a	2.651	0.254
O13a···X2	3.053	0.121
O13a···O3a	2.893	0.155
O13a···O7b	3.027	0.125
O13b···X1	3.049	0.122
O13b···O3b	2.903	0.152
O13b···O7a	3.024	0.126
O13b···O15b	2.785	0.189
O14a···O3b	2.753	0.202
O14a···O8b	2.814	0.179
O14a···O12a	2.723	0.215
O14b···O8a	2.779	0.192
O14b···O3a	2.781	0.191
O15a···O2b	2.884	0.157
O15b···O14a	3.118	0.111
O15b···A1	3.016	0.127
A1···O7a	2.720	0.217
A1–O15b	3.016	0.127

[1]from Ferraris and Ivaldi (1988).

paulkerrite-group mineral to have a co-dominant trivalent cation at the *M*1 sites. All previous members of the group have had either Mg or Mn^{2+} as the dominant cation at *M*1. The evidence for trivalent Fe^{3+} in sperlingite is indirect as there was insufficient material available for a direct determination of the valence state. Nevertheless, the bond distances and BVS values give strong support for trivalent Fe at *M*1. Using the Shannon (1976) ionic radii for 6-coordinated cations and 2-coordinated O^{2-} for the proposed site occupations in the empirical formula ($Mn^{2+}_{0.30}Mg_{0.165}Zn_{0.145}Fe^{n+}_{0.39}$), gives <*M*1–O> = 2.077 Å for Fe as Fe^{3+} and 2.149 Å for Fe^{2+}. These compare with the <*M*1a–O> and <*M*1b–O> values obtained from the refinement of 2.079 and 2.087 Å. Thus, the refined bond distances for the *M*1 sites give good indirect support to the site being occupied by a mix of large Mn^{2+} and small Fe^{3+}, together with minor Mg and Zn.

In all previous studies on paulkerrite-group minerals, valency variations occur only at the *A* sites (K^+, H_2O and vacancy), and the *M*2 and *M*3 sites (Fe^{3+}, Al^{3+} and Ti^{4+}). The species at all three sites coordinate to anions at the *X* sites, and so the charge balance in the structure can be maintained by variations in the ratio of univalent (F^- and OH^-) to divalent (O^{2-}) anions at *X*. Cations at the *M*1 site do not coordinate to anions at *X*, and so for sperlingite, with a mix of divalent and trivalent cations at *M*1, a different local charge balance mechanism is required. We have used the mechanism proposed by Hawthorne (1988) for sigloite, $Fe^{3+}[(H_2O)_3OH][Al_2(PO_4)_2(OH)_2(H_2O)_2]\cdot 2H_2O$, the oxidised analogue of paravauxite, $Fe^{2+}(H_2O)_4[Al_2(PO_4)_2(OH)_2(H_2O)_2]\cdot 2H_2O$. These laueite-group minerals have a $MO_2(H_2O)_4$ octahedron that is topologically identical to the *M*1-centred octahedra in sperlingite, and which is occupied by Fe^{2+} in paravauxite. When the Fe is oxidised to Fe^{3+} as in sigloite, the local charge balance is retained by replacement of H_2O that is coordinated to *M* by OH^-. Applying this mechanism to sperlingite gives a local charge balance when Fe^{3+} is present at the *M*1 site, by partial replacement of H_2O by OH^- at the octahedron. The four H_2O groups coordinating to *M*1 are O9 to O12, inclusive. As seen from Tables 5 and 7, the bond distances and BVS values are similar for the four coordinated *M*1–H_2O at both *M*1a and *M*1b sites suggesting that the OH^- replacement for H_2O is disordered over the four H_2O groups per octahedron.

Taking into account the mixed valence cations at *M*1 and the OH^- for H_2O substitution, the resulting ideal formula for sperlingite is $(H_2O)K(Mn^{2+}Fe^{3+})(Al_2Ti)(PO_4)_4[O(OH)][(H_2O)_9(OH)]\cdot 4H_2O$. The general formula for monoclinic paulkerrite-group minerals needs a revision to account for minerals like sperlingite, giving $A1A2(M1^{3+}_{n}M1^{2+}_{2-n})M2_2M3(PO_4)_4X_2(H_2O)_{10-n}(OH)_n\cdot 4H_2O$. Paulkerrite-group minerals described to date have $n = 0$, whereas sperlingite has $n = 1$.

Sperlingite is chemically and structurally most closely related to rewitzerite (Grey *et al*, 2023c) with the same dominant *A*, (*M*2$_2$*M*3) and *X* species. The properties of the two minerals are compared in Table 9.

Table 9. Comparison of rewitzerite and sperlingite.

	Rewitzerite	Sperlingite
Ideal formula	$K(H_2O)Mn_2(Al_2Ti)(PO_4)_4[O(OH)](H_2O)_{10}\cdot 4H_2O$	$(H_2O)K(Mn^{2+}Fe^{3+})(Al_2Ti)(PO_4)_4[O(OH)][(H_2O)_9(OH)]\cdot 4H_2O$
Crystal system	monoclinic	monoclinic
Space group	$P2_1/c$	$P2_1/c$
a (Å)	10.444(2)	10.428(2)
b (Å)	20.445(2)	20.281(4)
c (Å)	12.2690(12)	12.223(2)
β (°)	90.17(3)	90.10(3)
V (Å^3)	2619.8(6)	2585.0(8)
Z	4	4
Strongest lines in powder X-ray pattern *D* (*I*) (*hkl*)	10.26 (53) (020) 7.44 (55) ($\bar{1}$11) 6.16 (92) (002) 5.19 (40) (200) 3.958 (32) ($\bar{2}$31) 3.703 (57) ($\bar{2}$22) 3.111 (97) ($\bar{2}$51) 2.862 (100) (260)	10.236 (37) (020) 7.447 (5) (111) 6.176 (100) (002) 5.191 (35) (200) 3.964 (22) (231) 3.727 (41) ($\bar{2}$22) 3.101 (86) (251) 2.839 (43) (260)
D_{calc} (g·cm^{-3})	2.33	2.40
Opt. Character	biaxial (+)	biaxial (+)
α	1.585(2)	1.600(est.)
β	1.586(2)	1.615(5)
γ	1.615(2)	1.635(5)
$2V_{meas}$ (°)	25(2)	82.7 (calc.)
Reference	Grey *et al*. (2023c)	This study

Supplementary material. The supplementary material for this article can be found at https://doi.org/10.1180/mgm.2024.40.

Acknowledgements. This research was undertaken in part using the MX2 beamline at the Australian Synchrotron, part of ANSTO, and made use of the Australian Cancer Research detector.

Competing interests. The authors declare none.

References

Aragao D., Aishima J., Cherukuvada H., Clarken R., Clift M., Cowieson N.P., Ericsson D.J., Gee C.L., Macedo S., Mudie N., Panjikar S., Price J.R., Riboldi-Tunnicliffe A., Rostan R., Williamson R. and Caradoc-Davies T.T. (2018) MX2: a high-flux undulator microfocus beamline serving both the chemical and macromolecular crystallography communities at the Australian Synchrotron, *Journal of Synchrotron Radiation*, **25**, 885–891.

Bamberger C.E., Begun G.M. and MacDougall C.S. (1990) Raman spectroscopy of potassium titanates: Their synthesis, hydrolytic reactions and thermal stability. *Applied Spectroscopy*, **44**, 31–37.

Birch W.D., Grey I.E., Keck E., Mills S.J. and Mumme W.G. (2018) The Hagendorf Süd pegmatite: Australian-Bavarian collaboration on the characterization of new secondary phosphate minerals. *Australian Journal of Mineralogy*, **19**, 7–19.

Bosi F., Hatert F., Halenius U., Pasero M., Ritsuro M. and Mills S.J. (2019a) On the application of the IMA-CNMNC dominant-valency rule to complex mineral compositions. *Mineralogical Magazine,* **83**, 627–632.

Bosi F., Biagioni C. and Oberti R. (2019b) On the chemical identification and classification of minerals. *Minerals*, **9**, 591.

Demartin F., Pilati T., Gay H.D. and Gramaccioli C.M. (1993) The crystal structure of a mineral related to paulkerrite. *Zeitschrift fur Kristallographie*, **208**, 57–71.

Demartin F., Gay H.D., Gramaccioli C.M. and Pilati T. (1997) Benyacarite, a new titanium-bearing phosphate mineral species from Cerro Blanco, Argentina. *The Canadian Mineralogist*, **35**, 707–712.

Dowty E. (2004) *ATOMS for Windows, vsn 6.1*. Shape Software, Kingsport, USA.

Ferraris G. and Ivaldi G. (1988) Bond valence vs. bond length in O···O hydrogen bonds. *Acta Crystallographica*, **B44**, 341–344.

Fransolet A.-M., Oustriere P., Fontan F. and Pillard F. (1984) La mantienneite, une novelle espece minerale du gisement de vivianite d'Anloua, Cameroun. *Bulletin de Mineralogie*, **107**, 737–744.

Gagné O.C. and Hawthorne F.C. (2015) Comprehensive derivation of bond-valence parameters for ion pairs involving oxygen. *Acta Crystallographica*, **B71**, 562–578.

Grey I.E., Keck E., MacRae C.M., Glenn A.M., Mumme W.G., Kampf A.R. and Cashion J.D. (2018) Secondary Zn-bearing phosphate minerals associated with alteration of phosphophyllite at Hagendorf-Süd, Bavaria. *European Journal of Mineralogy*, **30**, 1007–1020.

Grey I.E., Hochleitner R., Rewitzer C., Kampf A.R., MacRae C.M., Gable R.W., Mumme W.G., Keck E. and Davidson C. (2023a) Pleysteinite, $[(H_2O)_{0.5}K_{0.5}]_2Mn_2Al_3(PO_4)_4F_2(H_2O)_{10}{\cdot}4H_2O$, the Al analogue of benyacarite, from the Hagendorf-Süd pegmatite, Oberpfalz, Bavaria, Germany. *European Journal of Mineralogy*, **35**, 189–197.

Grey I.E., Keck E., Kampf A.R., MacRae C.M., Gable R.W., Mumme W.G., Glenn A.M., and Davidson C. (2023b) Hochleitnerite, $[K(H_2O)]Mn_2(Ti_2Fe)(PO_4)_4O_2(H_2O)_{10}{\cdot}4H_2O$, a new paulkerrite-group mineral, from the Hagendorf-Süd pegmatite, Oberpfalz, Bavaria, Germany. *European Journal of Mineralogy*, **35**, 635–643.

Grey I.E., Hochleitner R., Kampf A.R., Boer S., MacRae C.M., Mumme W.G., and Keck E. (2023c) Rewitzerite, $K(H_2O)Mn_2(Al_2Ti)(PO_4)_4[O(OH)](H_2O)_{10}{\cdot}4H_2O$, a new monoclinic paulkerrite-group mineral, from the Hagendorf Süd pegmatite, Oberpfalz, Bavaria, Germany. *Mineralogical Magazine*, **87**, 830–838.

Grey I.E., Boer S., MacRae C.M., Wilson N.C., Mumme W.G. and Bosi F. (2023d) Crystal chemistry of type paulkerrite and establishment of the paulkerrite group nomenclature. *European Journal of Mineralogy*, **35**, 909–919.

Grey I.E., Rewitzer C., Hochleitner Kampf A.R., Boer S., Mumme W.G.. and Wilson N.C. (2024) Macraeite, $[(H_2O)K]Mn_2(Fe_2Ti)(PO_4)_4[O(OH)](H_2O)_{10}{\cdot}4H_2O$, a new monoclinic paulkerrite-group mineral from the Cubos-Mesquitela-Mangualde pegmatite, Portugal, *European Journal of Mineralogy*, **36**, 267–278.

Hawthorne F.C. (1985) Towards a structural classification of minerals: The $^{vi}M^{iv}T_2\Phi_n$ minerals. *American Mineralogist*, **70**, 455–473.

Hawthorne. F.C. (1988) Sigloite: The oxidation mechanism in $[M_2^{3+}(PO_4)_2(OH)_2(H_2O)_2]^{2-}$ structures. *Mineralogy and Petrology*, **38**, 201–211.

Hochleitner R., Grey I.E., Kampf A.R., Boer S., MacRae C.M., Mumme W.G. and Wilson N.C. (2024) Fluor-rewitzerite, $[(H_2O)K]Mn_2(Al_2Ti)(PO_4)_4[OF](H_2O)_{10}{\cdot}4H_2O$, a new paulkerrite-group mineral, from the Hagendorf Süd pegmatite, Oberpfalz, Bavaria, Germany. *European Journal of Mineralogy*, **36**, 541–554.

Kabsch W. (2010) *XDS. Acta Crystallographica*, **D66**, 125–132.

Kastning J. and Schlüter J. (1994) *Die Mineralien von Hagendorf und ihre Bestimmung*. Schriften des Mineralogischen Museums der Universität Hamburg, Band 2, C. Weise Verlag, Munich, 95 pp.

Libowitzky E. (1999) Correlation of O–H stretching frequencies and O–H···O hydrogen bond lengths in minerals. *Monatschefte fűr Chemie*, **130**, 1047–1059.

Mills S.J., Grey I.E., Kampf A.R., Birch W.D., MacRae C.M., Smith J.B. and Keck E. (2016) Kayrobertsonite, $MnAl_2(PO_4)_2(OH)_2{\cdot}6H_2O$, a new phosphate mineral related to nordgauite. *European Journal of Mineralogy*, **29**, 649–654.

Mücke A. (1981) The paragenesis of the phosphate minerals of the Hagendorf pegmatite — a general view. *Chemie der Erde*, **40**, 217–234.

Peacor D.R., Dunn P.J. and Simmons W.B. (1984) Paulkerrite a new titanium phosphate from Arizona. *The Mineralogical Record*, **1984**, 303–306.

Petříček V., Dušek M. and Palatinus L. (2014) Crystallographic Computing System JANA2006: General features. *Zeitschrift fur Kristallographie*, **229**, 345–352.

Pouchou J.L. (1993) X-ray microanalysis of stratified specimens. *Analytica Chimica Acta*, **283**, 81–97.

Rewitzer C., Hochleitner R., Grey I.E., Kampf A.R., Boer S., MacRae C.M., Mumme W.G., Wilson N.C. and Davidson C. (2024a) Sperlingite, IMA 2023-120. CNMNC Newsletter 78. *Mineralogical Magazine*, **88**, 345–349, https://doi.org/10.1180/mgm.2024.23

Rewitzer C., Hochleitner R., Grey I.E., MacRae C.M., Mumme W.G., Boer S., Kampf A.R. and Gable R.W. (2024b) Monoclinic pleysteinite and hochleitnerite from the Hagendorf Süd pegmatite. Synchrotron microfocus diffraction studies on paulkerrite-group minerals. *The Canadian Journal of Mineralogy and Petrology*, **62**, 513–527.

Schaaf P., Sperling T. and Müller-Sohnius D. (2008) Pegmatites from the Bavarian Forest, SE Germany: Geochronology, Geochemistry and Mineralogy. *Geologica Bavarica*, **110**, 204–303 and 420—429.

Sejkora J., Skoda R., Ondrus P., Beran P. and Susser C. (2006) Mineralogy of phosphate accumulations in the Huber stock, Krasno ore district, Slavkovsky les area, Czech Republic, *Journal of the Czech Geological Society*, **51**, 103—147.

Shannon R.D. (1976) Revised effective ionic radii and systematic studies of interatomic distances in halides and chalcogenides. *Acta Crystallographica*, **A32**, 751—767.

Sheldrick G.M. (2015) Crystal-structure refinement with SHELX. *Acta Crystallographica*, **C71**, 3–8.

Silva F.L.R., Filho A.A.A., Silva M.B., Balzuweit K., Bantiignies J-L., Caetano E.W.S., Moreira R.L., Freire V.N. and Righi A. (2018) Polarized Raman, FTIR, and DFT study of Na2Ti3O7 microcrystals. *Journal of Raman Spectroscopy*, **49**, 535–548.

Sperling T. (2000) The geological mapping of Bavaria under the leadership of Carl Wilhelm von Gümbel. *Third congress on regional cartography and information systems (Munich, October 24th - 27th, 2000)*, Proceedings: pp. 299–302; München.

Tu C.-S., Guo A.R., Tao R., Katiyar R.S., Guo R. and Bhalla A.S. (1996) Temperature dependent Raman scattering in $KTiOPO_4$ and $KTiOAsO_4$ single crystals. *Journal of Applied Physics*, **79**, 3235–3240.

Wright S.E., Foley J.A. and Hughes J.M. (2000) Optimisation of site occupancies in minerals using quadratic programming. *American Mineralogist*, **85**, 524–531.

https://doi.org/10.1180/mgm.2024.40 Published online by Cambridge University Press